Electronic Supplementary Material (ESI)

for

Multivariate Indium-Organic Frameworks for Highly Efficient Carbon Dioxide Capture and Electrocatalytic Conversion

Shuo Wang, Ying Wang, Jia-Min Huo, Wen-Yu Yuan*, Peng Zhang, Shu-Ni Li, and Quan-Guo Zhai*

Key Laboratory of Macromolecular Science of Shaanxi Province, Key Laboratory of Applied Surface and Colloid Chemistry, Ministry of Education, School of Chemistry & Chemical Engineering, Shaanxi Normal University, Xi'an, Shaanxi, 710062, China.
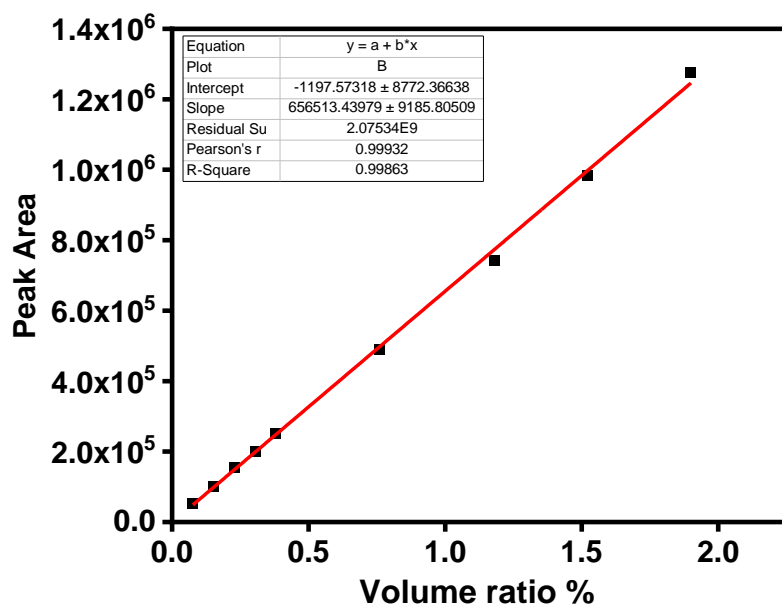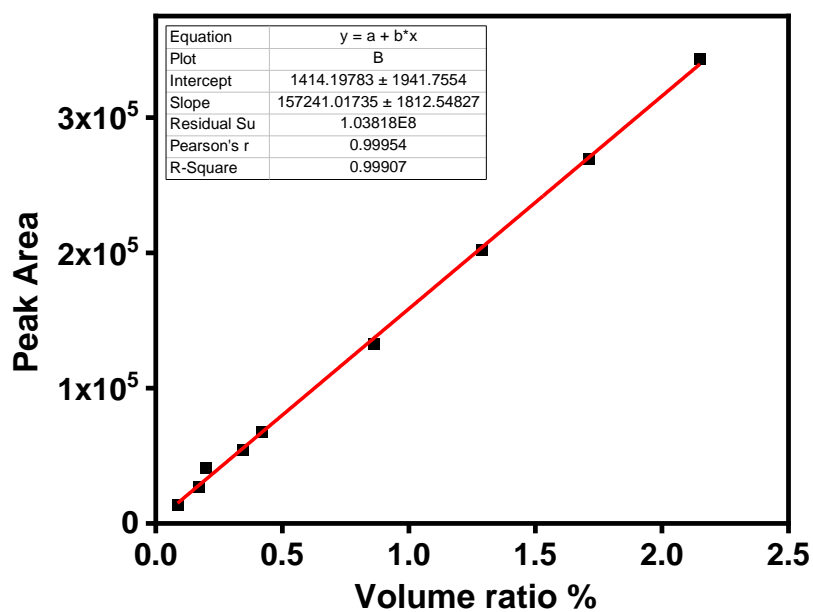
Section S1. Standard curves

Equation	y = a + b*x
Plot	B
Intercept	-1197.57318 ± 8772.36638
Slope	656513.43979 ± 9185.80509
Residual Su	2.07534E9
Pearson's r	0.99932
R-Square	0.99863

Fig. S1 Standard curve of H_2.

Equation	y = a + b*x
Plot	B
Intercept	1414.19783 ± 1941.7554
Slope	157241.01735 ± 1812.54827
Residual Su	1.03818E8
Pearson's r	0.99954
R-Square	0.99907

Fig. S2 Standard curve of CO.

Equation	y = a + b*x
Plot	B
Intercept	0 ± --
Slope	0.00191 ± 4.01608E-5
Residual Sum	1.20967E-6
Pearson's r	0.99911
R-Square	0.99823
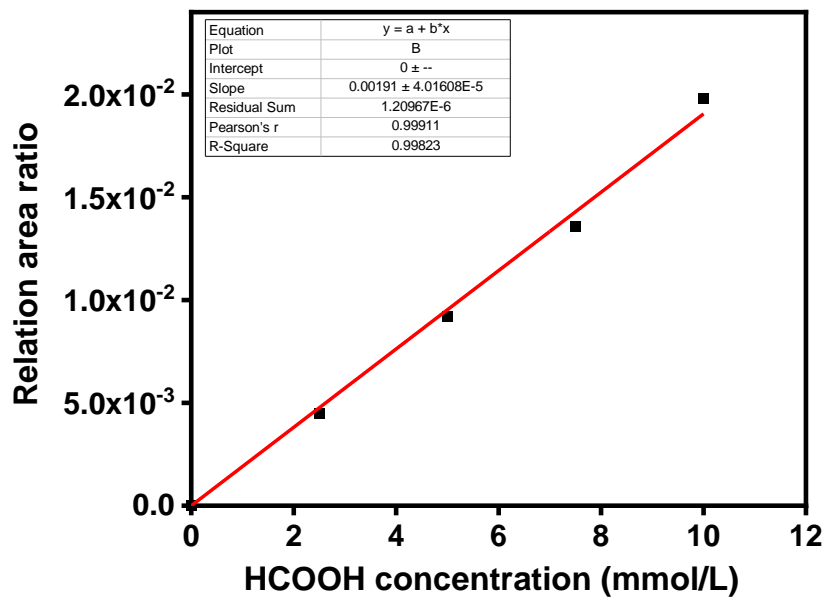
Fig. S3 Standard curve of HCOOH.

Section S2. Supplementary figures and tables
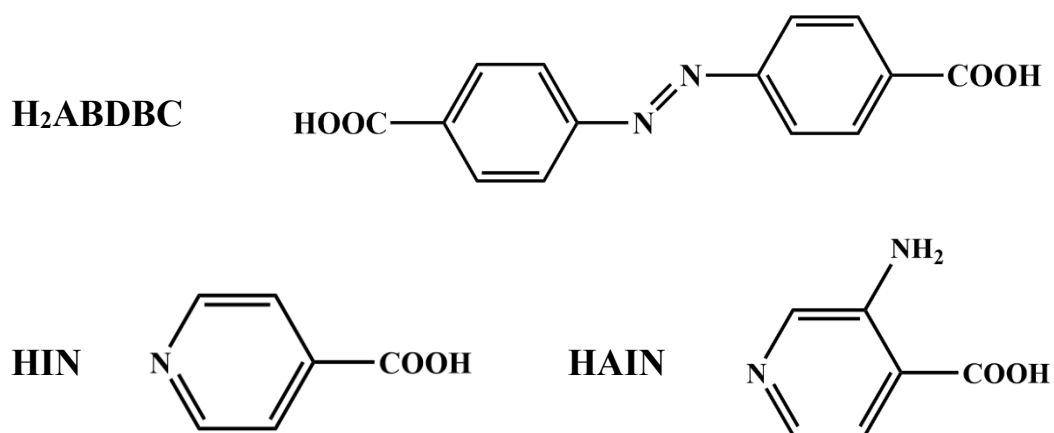
H₂ABDBC

HIN

HAIN

Fig. S4 View of the structure of H₂ABDBC, HIN and HAIN.
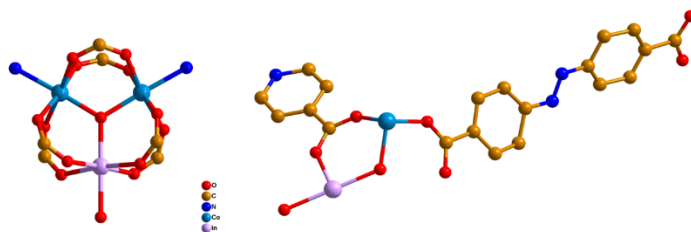

Fig. S5 Structure of the InCo₂ cluster and asymmetric unit.
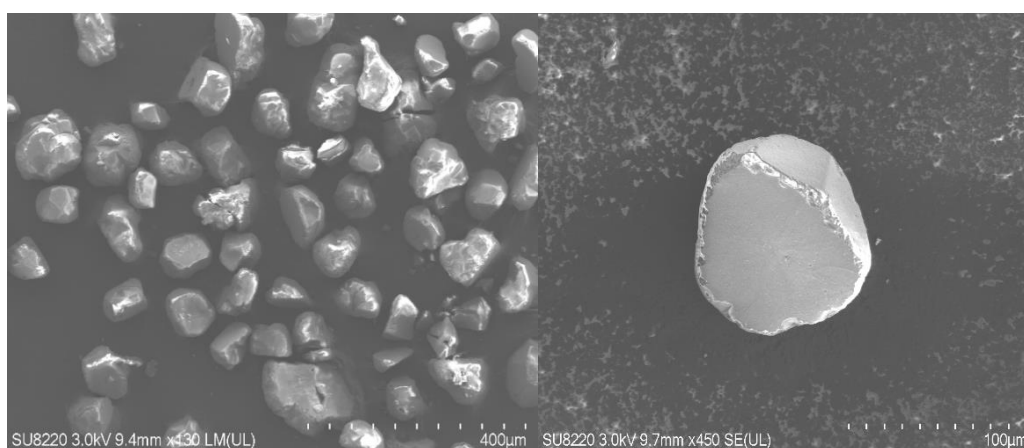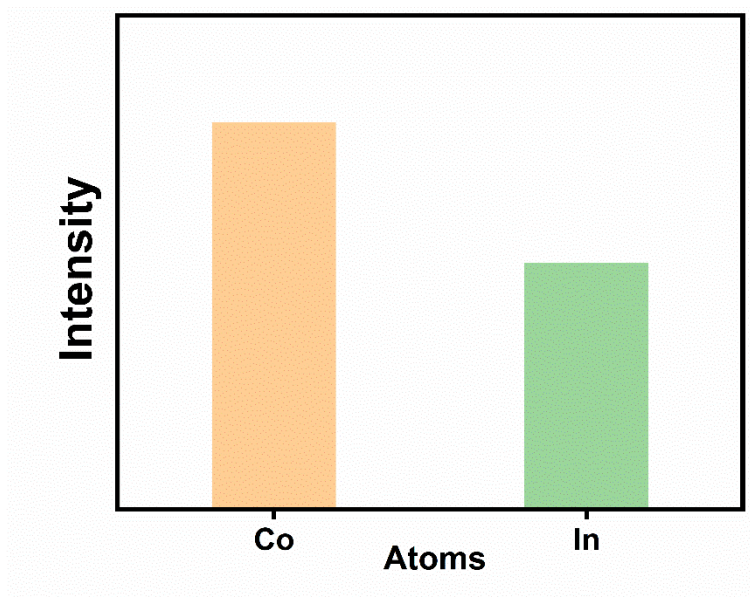

Fig. S6 SEM of InCo-ABDBC-HIN.

Fig. S7 The atomic ratio of In:Co (1:1.6) of InCo-ABDBC-HIN from ICP-MS analysis.
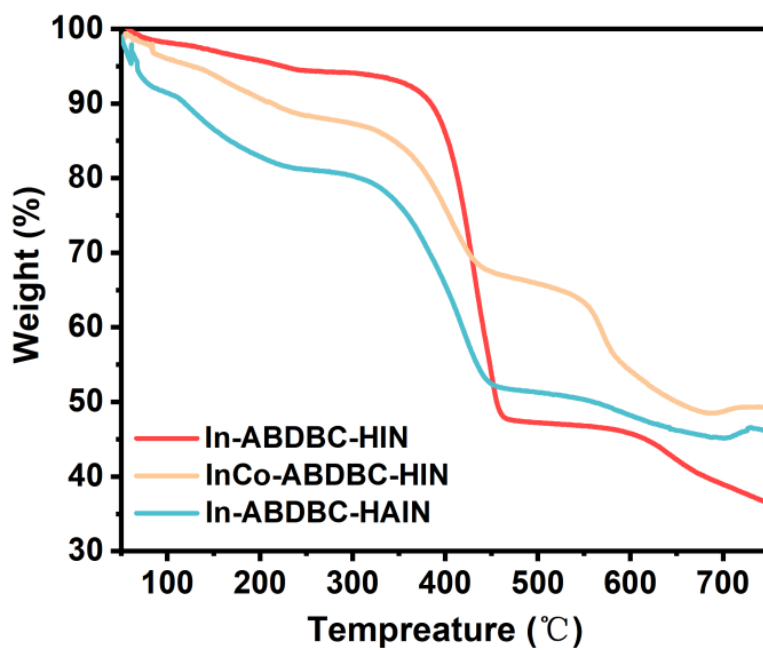

Fig. S8 Thermogravimetric analyses (TGA) curves for synthesized In-ABDBC-HIN, InCo-ABDBC-HIN and In-ABDBC-HAIN.
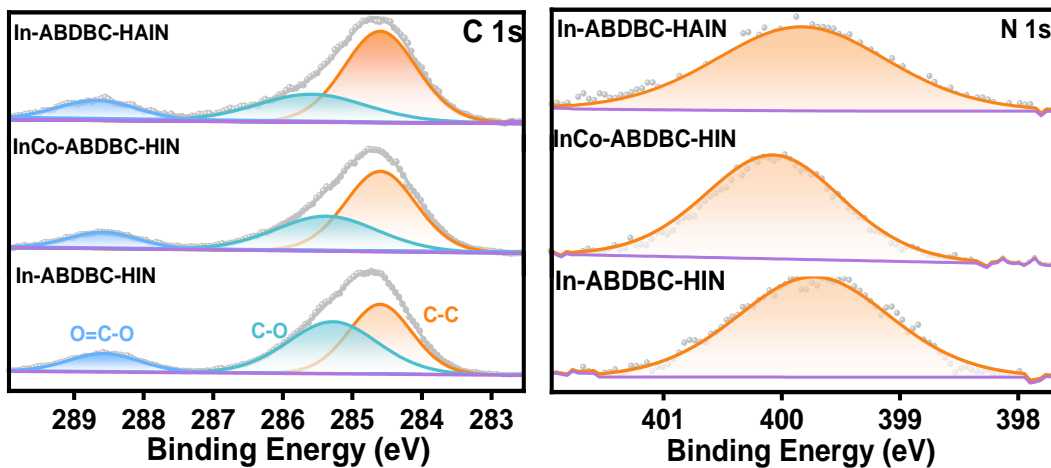
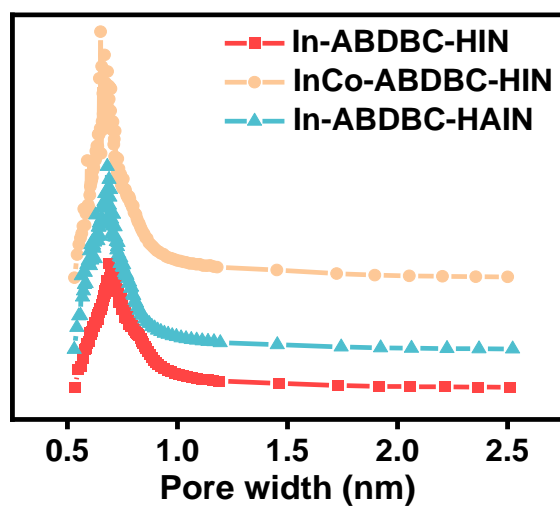**Fig. S9** (a) C 1s and (b) N1s XPS spectra for In-ABDBC-HIN, InCo-ABDBC-HIN and In-ABDBC-HAIN.

Fig. S10 Pore size distribution calculated using the Horvath−Kawazoe method of In-ABDBC-HIN, InCo-ABDBC-HIN and In-ABDBC-HAIN.
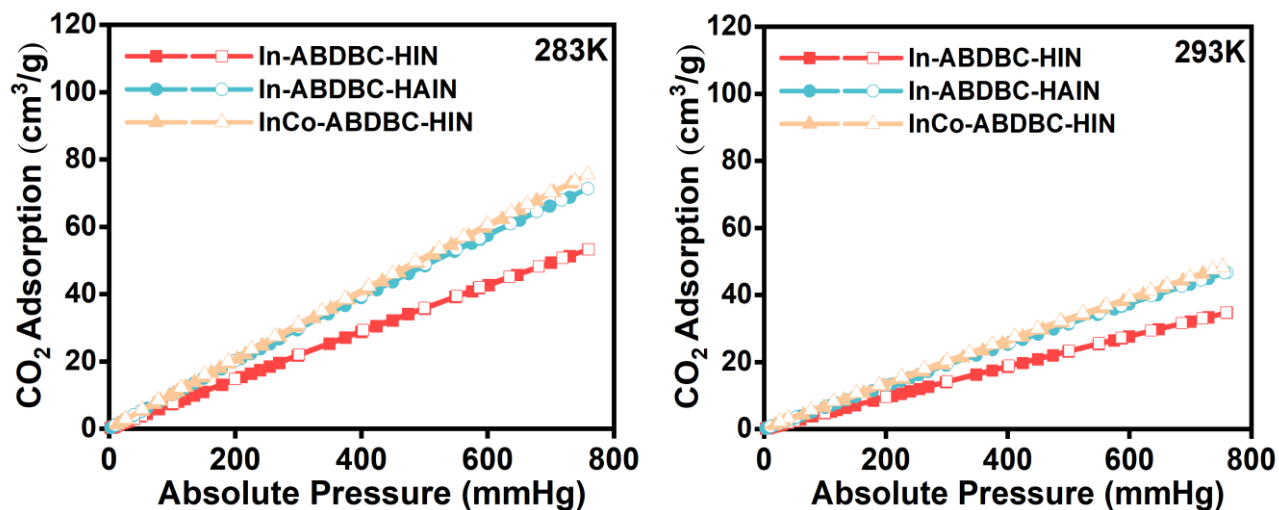
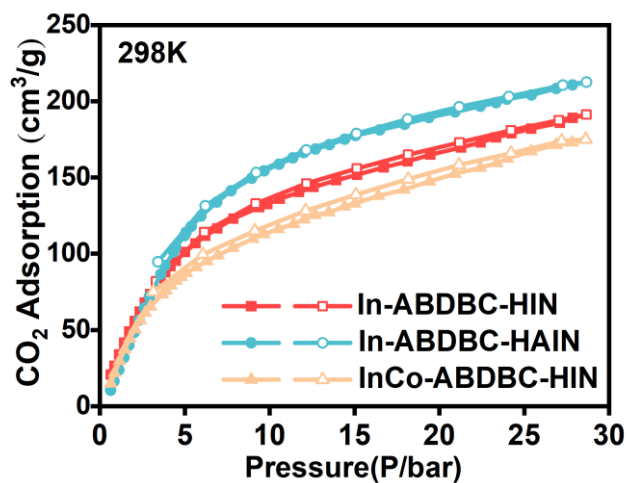**Fig. S11** Low-pressure CO_2 adsorption isotherms at 283K, 298K.

Fig. S12 High-pressure CO_2 adsorption isotherms at 298 K.
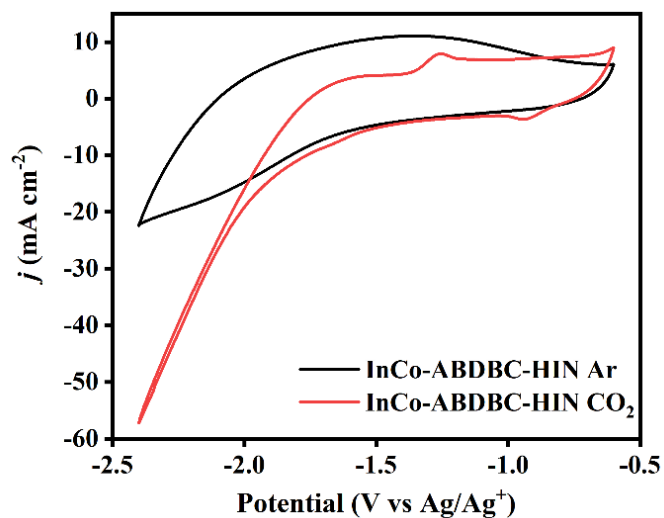
Fig. S13 CV of In-ABDBC-HIN in N_2- and CO_2-saturated electrolytes.
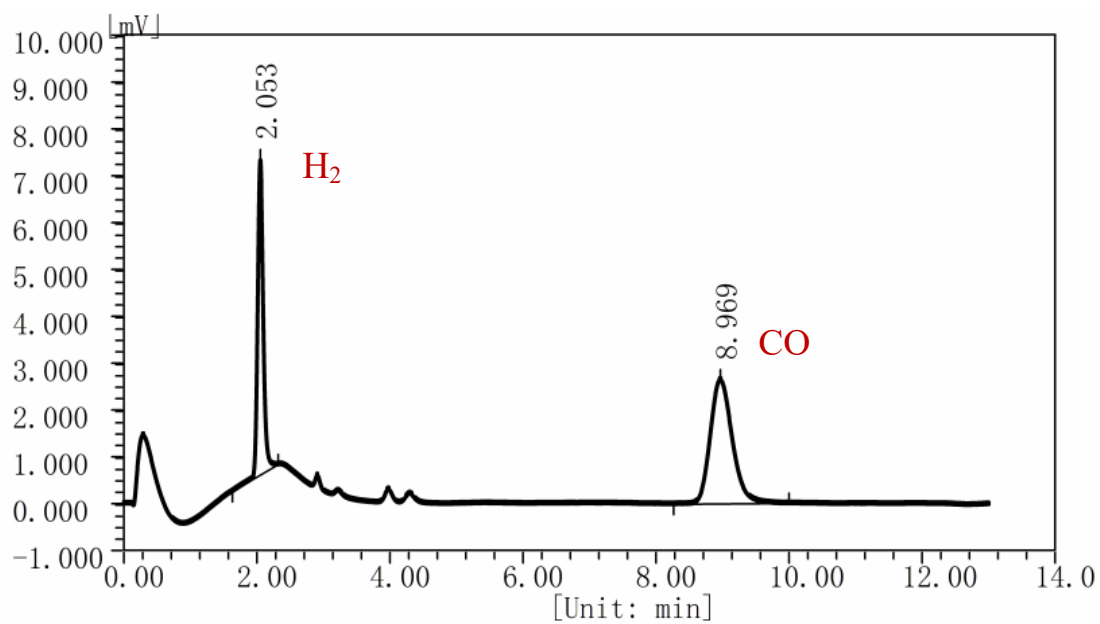
Fig. S14 Characterization of products by gas chromatography (GC).
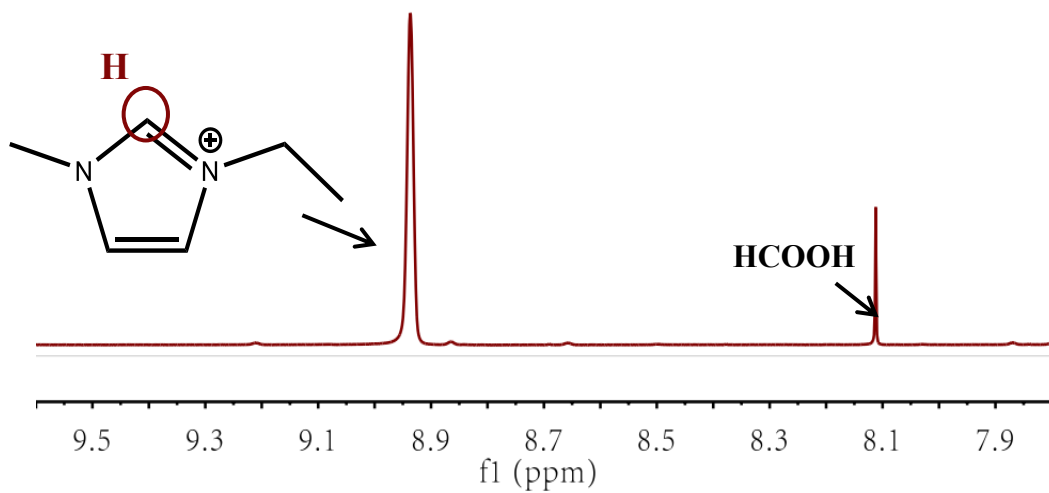
Fig. S15 Characterization of products by 1H NMR spectroscopy.
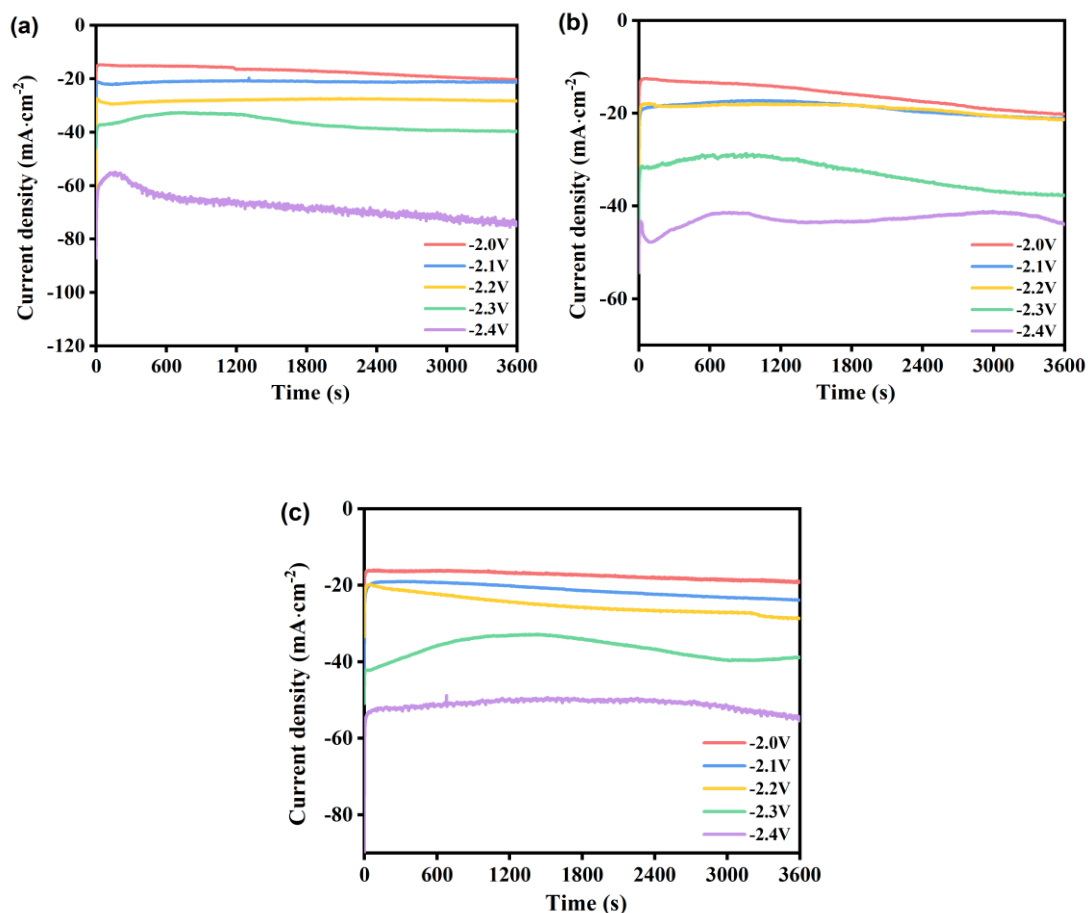
Fig. S16 Potentiostatic current density vs. time curves of CO$_2$RR under the condition for (a) In-ABDBC-HIN, (b) InCo-ABDBC-HIN and (c) In-ABDBC-HAIN.
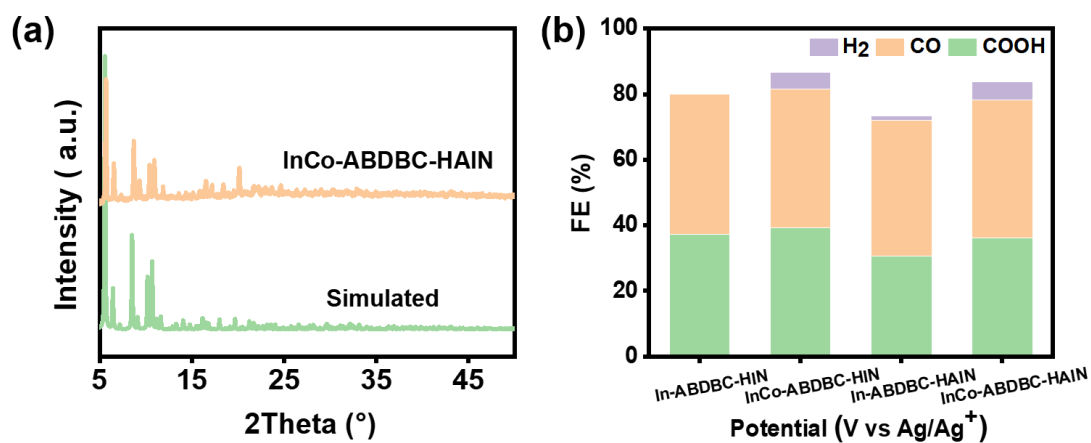
Fig. S17 (a) XRD pattern of InCo-ABDBC-HAIN and (b) the Faraday efficiency of In-ABDBC-HIN, InCo-ABDBC-HIN, In-ABDBC-HAIN and InCo-ABDBC-HAIN at -2.2 V (vs Ag/Ag$^+$).
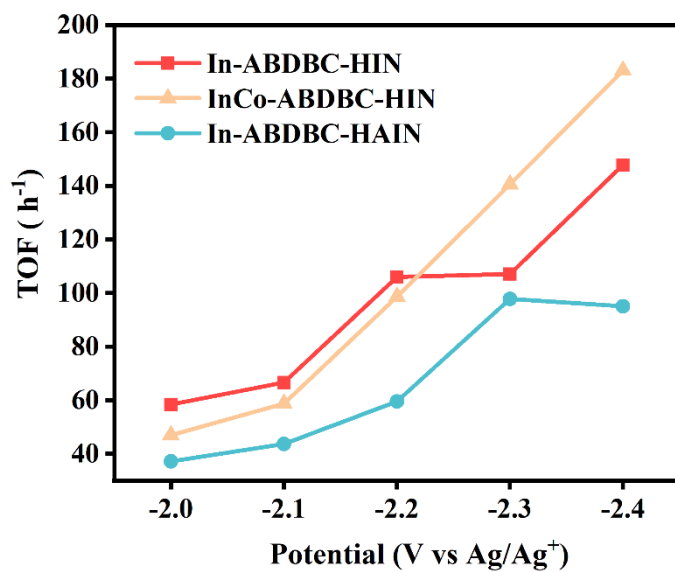
Fig. S18 TOF plots for the generation of C_1 products.
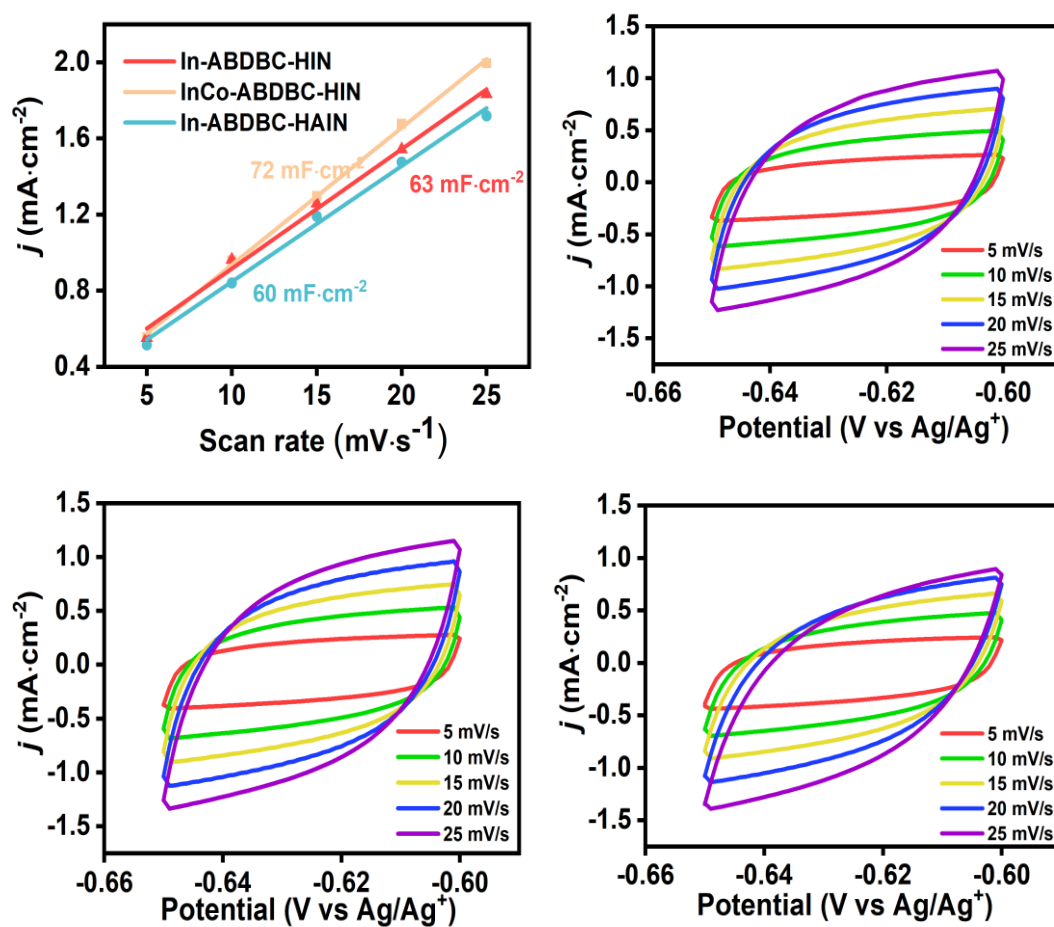
Fig. S19 ECSA of In-ABDBC-HIN, InCo-ABDBC-HIN and In-ABDBC-HAIN.
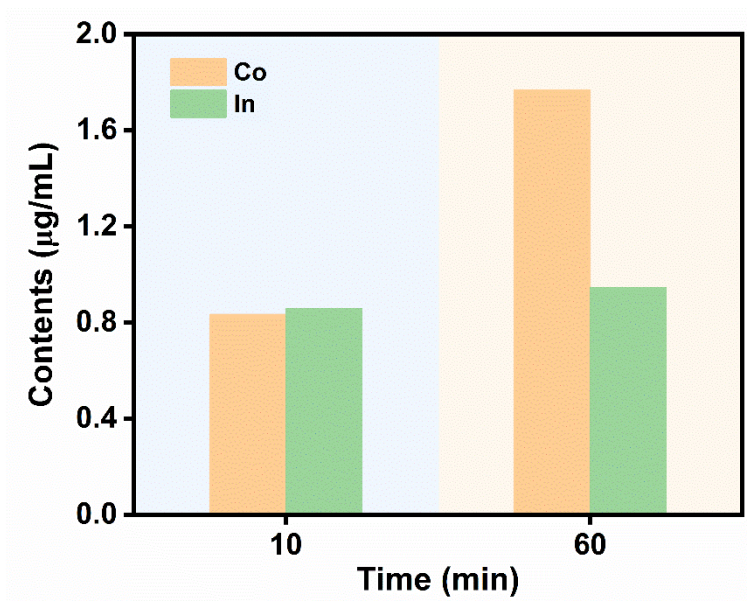
Fig. S20 The dissolution of metal elements in the electrolyte during continuous electrocatalysis under a potential of -2.2 V vs Ag/Ag$^+$.
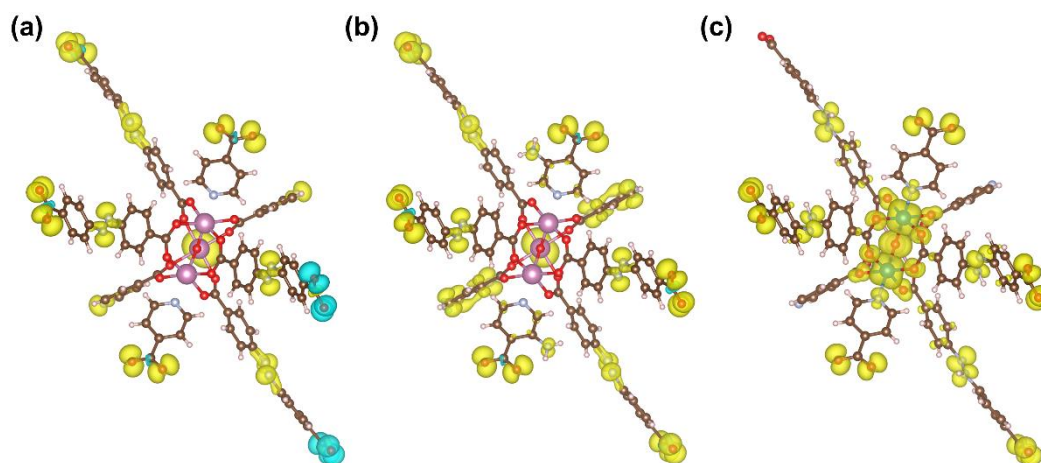
Fig. S21 The top-view of the structure for DFT calculations and the distribution of unpaired electrons for (a) In-ABDBC-HIN, (b) In-ABDBC-HAIN, and (c) InCo-ABDBC-HIN.

Table S1. Crystal data and structure refinements for InCo-ABDBC-HIN

Compound	InCo-ABDBC-HIN
Empirical formula	$C_{40}H_{27}Co_2InN_6O_{14}$
Formula weight	1049.36
Crystal system	Cubic
Space group	I-43d
a (Å)	38.2668(4)
b (Å)	38.2668(4)
c (Å)	38.2668(4)
α (°)	90
β (°)	90
γ (°)	90
Volume ($Å^3$)	56036.1(19)
Z	24
ρ_{calc}g/cm^3	0.746
μ (mm^{-1})	0.630
F(000)	12600.0
2θ range for data collection (°)	3.982 to 61.214
Reflections collected/unique	45055/12346
R_{int}	0.0540
Parameters	288
Goodness-of-fit on F^2	1.000
R_1[a], ωR_2 [I>=2δ (I)]	R_1 = 0.0347, ωR_2 = 0.0857
R_1, ωR_2 (all data)	R_1 = 0.0493, ωR_2 = 0.0903
ρ_{fin} (max/min) (e Å^{-3})	0.35/-0.54

Table S2. Selected bonded lengths (Å) and angles (°) for InCo-ABDBC-HIN

In(1)-O(1)	2.088(4)	O(1)-Co(1)[(#3)]	2.0353(19)
In(1)-O(7) [(#1)]	2.135(3)	C(3)-C(2)	1.339(5)
In(1)-O(7)[(#2)]	2.135(3)	C(3)-C(4)	1.387(5)
In(1)-O(8)	2.141(4)	C(7)-C(8)	1.488(5)
In(1)-O(2)[(#3)]	2.195(3)	C(2)-C(6)	1.393(5)
In(1)-O(2)	2.195(3)	C(2)-C(1)	1.525(5)
Co(1)-O(1)	2.0354(19)	C(6)-C(5)	1.379(5)
Co(1)-O(4)	2.088(3)	C(8)-C(9)	1.381(6)
Co(1)-O(5)[(#3)]	2.091(3)	C(8)-C(13)	1.423(6)
Co(1)-O(6)[(#1)]	2.101(3)	C(17)-C(16)	1.305(7)
Co(1)-O(3)	2.122(2)	C(17)-C(18)	1.367(7)
Co(1)-N(1)[(#4)]	2.164(3)	C(17)-C(20)	1.513(5)
O(4)-C(7)	1.250(4)	C(14)-C(15)	1.233(8)
O(5)-C(7)	1.267(5)	C(14)-N(3)	1.411(6)
O(5)-Co(1)[(#3)]	2.090(3)	C(14)-C(19)	1.454(9)
O(3)-C(1)	1.245(4)	C(13)-C(12)	1.418(6)
N(1)-C(4)	1.318(4)	C(9)-C(10)	1.344(7)
N(1)-C(5)	1.366(4)	C(11)-C(12)	1.264(9)
N(1)-Co(1)[(#5)]	2.164(3)	C(11)-C(10)	1.485(9)
O(2)-C(1)	1.231(4)	C(11)-N(2)	1.522(7)
O(6)-C(20)	1.262(5)	N(3)-N(2)	1.264(7)
O(6)-Co(1)[(#6)]	2.101(3)	C(16)-C(15)	1.402(7)
O(7)-C(20)	1.255(5)	C(19)-C(18)	1.395(7)
O(7)-In(1)[(#7)]	2.135(3)		

Symmetry (#1)1/4+X,3/4-Z,5/4-Y; (#2)3/4-X,-1/4+Z,5/4-Y; (#3)1-X,1/2-Y,+Z; (#4)-1/2+Z,1/2-X,1-Y; (#5)1/2-Y,1-Z,1/2+X; (#6)-1/4+X,5/4-Z,3/4-Y; (#7)3/4-X,5/4-Z,1/4+Y

Table S3. Comparison of various In-MOF catalysts for CO_2 electroreduction

Catalysts	electrolyte	Current density (mA·cm^{-2})	Main products	FE$_{C1}$ (%)	Ref.
InCo-ABDBC-HIN	0.5 M EMIMBF$_4$	26	HCOOH + CO	81.60	
In-ABDBC-HIN	0.5 M EMIMBF$_4$	25	HCOOH + CO	79.97	This work
In-ABDBC-HAIN	0.5 M EMIMBF$_4$	19	HCOOH + CO	71.94	
In-BDC	0.5M KHCO$_3$	6.49	HCOOH + CO	100.00	[1]
MFM-300(In)-e/In	0.5 M EMIMBF$_4$	46.1	HCOOH	99.10	[2]
MFM-300(In)-t/CP	0.5 M EmimBF$_4$	28.4	HCOOH	68.10	[2]
MFM-300(In)-e/CP	0.5 M EmimBF4	28	HCOOH	81.50	[2]
(Me$_2$NH$_2^+$){In^{III}-[Ni(C$_2$S$_2$(C$_6$H$_4$COO)$_2$)$_2$]}·3DMF·1.5H$_2$O	0.5 M KHCO$_3$	36	HCOOH + CO	91.47	[3]
(Me$_2$NH$_2^+$)[In^{III}-(TTFTB)] • 0.7C$_2$H$_5$OH • DMF	0.5 M KHCO$_3$	14.3	HCOOH + CO	60.17	[3]
MIL-68(In)-NH2	0.1M KHCO$_3$	108	HCOOH	94.40	[4]
CPs@V11	0.5 M KHCO$_3$	6.87	HCOOH	90.30	[5]
V11	0.5 M KHCO$_3$	2.97	HCOOH	72.20	[5]
PF-110	0.5 M KHCO$_3$	2.97	HCOOH	64.00	[5]
ZJU-28	0.5 M KHCO$_3$	2.28	HCOOH	58.00	[5]
MIL-68	0.5 M KHCO$_3$	0.94	HCOOH	54.00	[5]
CPM-5	0.5 M KHCO$_3$	0.75	HCOOH	39.50	[5]

Section S3. References

[1] S. Z. Hou, X. D. Zhang, W. W. Yuan, Y. X. Li and Z. Y. Gu, Indium-Based Metal-Organic Framework for High-Performance Electroreduction of CO_2 to Formate, *Inorg. Chem.*, 2020, **59**, 11298-11304.

[2] X. Kang, B. Wang, K. Hu, K. Lyu, X. Han, B. F. Spencer, M. D. Frogley, F. Tuna, E. J. L. McInnes, R. A. W. Dryfe, B. Han, S. Yang and M. Schroder, Quantitative Electro-Reduction of CO_2 to Liquid Fuel over Electro-Synthesized Metal-Organic Frameworks, *Angew. Chem. Int. Ed.*, 2020, **142**, 17384-17392.

[3] Y. Zhou, S. Liu, Y. Gu, G. H. Wen, J. Ma, J. L. Zuo and M. Ding, In(III) Metal-Organic Framework Incorporated with Enzyme-Mimicking Nickel Bis(dithiolene) Ligand for Highly Selective CO_2 Electroreduction, *Angew. Chem. Int. Ed.*, 2021, **143**, 14071-14076.

[4] Z. Wang, Y. Zhou, C. Xia, W. Guo, B. You and B. Y. Xia, Efficient Electroconversion of Carbon Dioxide to Formate by a Reconstructed Amino-Functionalized Indium-Organic Framework Electrocatalyst, *Angew. Chem. Int. Ed.*, 2021, **60**, 19107-19112.

[5] Z. H. Zhu, B. H. Zhao, S. L. Hou, X. L. Jiang, Z. L. Liang, B. Zhang and B. Zhao, A Facile Strategy for Constructing a Carbon-Particle-Modified Metal-Organic Framework for Enhancing the Efficiency of CO_2 Electroreduction into Formate, *Angew. Chem. Int. Ed.*, 2021, **60**，23394-23402.